Comparative analysis of four different fly ash sources as additives in porcelain ceramics: microstructural and mechanical characterization

I. Erdogana, H. Kursuna, U. Onenb, T. Boyraza and T. Kursunc

Porcelain is a non-porous, vitrified ceramic material characterized by a white, fine-grained, and often semi-transparent body. Its superior toughness, strength, and translucency compared to other ceramic types are primarily attributed to the vitrification process and the formation of mullite phases within the body. Fly ash is a by-product collected by electrostatic precipitators in coal-fired power plants. Due to its rich elemental composition and often alkaline nature, fly ash is commonly utilized as an additive in the production of various ceramic materials. In this study, the effects of fly ash from different thermal power plants—Çatalağzı-Zonguldak (ÇAT), Çayırhan-Ankara (ÇAY), Kangal-Sivas (KAN), and Afşin-Elbistan A (AFŞ)—on the properties of porcelain bodies were investigated. To this end, commercial porcelain bodies were modified by incorporating 0%, 15%, and 30% fly ash by weight into the compositions. The powder mixtures were homogenized by ball milling at 75 rpm for 24 hours and then shaped via uniaxial dry pressing at 100 MPa. The pressed samples were subsequently fired at temperatures ranging from 1050 °C to 1150 °C for 1 hour. Comprehensive analyses were conducted on the resulting porcelain bodies, including microstructural evaluation (SEM), phase analysis (XRD), mechanical testing (three-point bending), and assessments of various physical properties such as color, linear shrinkage, water absorption, apparent porosity, and bulk density. Among the tested samples, the composition containing 15 wt.% ÇAT fly ash and fired at 1150 °C exhibited the best performance, with a compressive strength of 20.58 MPa and a water absorption rate below 0.5%. The results suggest that selected fly ash types can enhance porcelain properties while supporting waste valorization.

Keywords: Porcelain, Fly ash, Ceramic properties, Waste valorization, Sintering behavior.

Introduction

Porcelain is a traditional ceramic material widely utilized in household applications and scientific and engineering fields. Its key technological attributes include high mechanical strength, low water absorption, translucency, and long-term durability [1–4]. Typically, porcelain bodies are composed of clay, feldspar, quartz, and other additives to achieve desired performance characteristics [1,2]. Clay imparts plasticity during shaping, while feldspar acts as a fluxing agent, promoting glass phase formation by reacting with the amorphous silica in clay and lowering the sintering temperature. The final sintered porcelain body predominantly consists of mullite, glassy phases, and quartz [1,3,5].

Mullite begins to form when porcelain is fired above 1100 °C and remains stable within the temperature range of 1200–1400 °C [6–8]. The formation of a viscous glass phase also occurs within this range, with the onset temperature depending on the chemical composition of

influence of pure oxides such as MgO and TiO_2 and industrial by-products like fly ash and ceramic waste on the properties of porcelain bodies [14–18]. Fly ash is a by-product produced during the combustion of coal in thermal power plants [19,20]. Its physical and chemical characteristics vary based on the origin of the coal and the combustion process used at the power plant [21]. Fly ash is an inorganic material with a particle size generally smaller than 100 μ m.

the porcelain. For instance, eutectic melting begins at approximately 990 °C for potash feldspar and around

1050 °C for soda feldspar. Developing a continuous

glassy matrix typically occurs between 1200 and

1400 °C [8,9]. Quartz dissolution becomes significant

at temperatures above 1200 °C and increases with both

temperature and dwell time, regardless of the heating

rate [7,10-13]. Numerous studies have examined the

The physical properties of fly ash include fineness (particle size), particle shape, specific surface area, and specific gravity. It primarily comprises fine spherical particles but may also contain irregular, angular fragments. Particle size distribution depends on the coal source and is commonly determined using dry and wet sieving techniques. Various analytical methods—such as

 $* Corresponding \ author:\\$

Tel: +90 3464870000/1689 Fax: +903462191165

E-mail: hlykursun@gmail.com / hkursun@cumhuriyet.edu.tr

^aDepartment of Metallurgical and Materials Engineering, Sivas Cumhuriyet University Sivas, Türkiye

^bDepartment of Metallurgical and Materials Engineering, Mersin University, Mersin, Türkiye

^cDepartment of Manufacturing Engineering Sivas Cumhuriyet University Sivas, Türkiye

X-ray micrography, laser particle size analysis, Coulter counter, Brunauer–Emmett–Teller (BET) surface area measurement, and the Blaine technique—are employed to assess surface area and particle size characteristics [21–26]. The specific gravity of fly ash can vary significantly among sources [27]. Chemically, fly ash predominantly contains silica, alumina, iron, calcium, magnesium, sulfur, carbon, titanium, and trace elements. It is produced through pulverized coal combustion at temperatures near 1200 °C and collected via electrostatic precipitators installed in power plant chimneys [28,29].

Numerous researchers have highlighted the key areas for fly ash utilization. Prominent applications include its use in the construction sector for producing bricks, blocks, tiles, cement, concrete, and plaster; in land reclamation and the filling of low-lying areas; for raising ground levels, constructing roads, embankments, ash dykes, roadblocks, and curbstones; as well as in the ceramic industry to produce bricks, floor tiles, sanitary ware, porcelain, and ceramic glazes. Additionally, fly ash has found use in agriculture, wasteland development, various industrial applications, high-value engineering sectors, hydroelectric projects, irrigation systems, drainage channels, and for lining rivers, tributaries, canals, roller-compacted dams, and pavements [30–37].

The ceramic industry is one of the largest consumers of natural raw materials. Globally, there is a growing emphasis on incorporating industrial waste materials as both an economically viable alternative and a strategy to mitigate environmental pollution [38]. Accordingly, significant research efforts have been directed toward using fly ash in ceramics. For instance, Kockal [39] examined the influence of different types of fly ash—used as a feldspar substitute—and varying sintering temperatures on the properties of sintered ceramic tile bodies, demonstrating its potential as a cost-effective aluminosilicate source. Other researchers have explored the partial replacement of traditional materials with fly ash in developing ceramic tiles [40–43].

Due to their exceptional properties—such as a high strength-to-weight ratio, high hardness, low density, excellent wear, and chemical resistance—ceramics have secured a crucial role in modern industrial applications [44,45]. Many researchers have conducted studies using different raw materials to create porcelain. These studies examined the compatibility of different raw materials with the porcelain structure and explored the use of alternative raw materials [46-55].

However, due to production complexity and cost, these properties also constrain their widespread use. Recently, considerable attention has been devoted to applying fly ash in the ceramic industry to address such limitations [41,56–61].

In the present study, the effects of fly ash sourced from four different thermal power plants—Çatalağzı (ÇAT), Çayırhan (ÇAY), Kangal (KAN), and Afşin-Elbistan A (AFŞ)—were investigated as additives in porcelain

ceramic compositions at proportions of 0%, 15%, and 30% by weight. The sintered samples were evaluated for density, porosity, shrinkage, and water absorption. Additionally, their microstructural and thermal properties were comprehensively analyzed.

Experimental Procedure

Characterization of raw materials

The materials utilized in this study include fly ash and commercial porcelain powder. Fly ash samples were obtained from four different thermal power plants: Çatalağzı (ÇAT), Çayırhan (ÇAY), Kangal (KAN), and Afşin-Elbistan A (AFŞ). Ready-made porcelain bodies were sourced from Refsan, located in Kütahya. The chemical compositions of both the fly ash and porcelain powder are presented in Table 1.

All powder mixtures were prepared using a ball-to-powder-to-water ratio of 3:1:1 by weight. The mixtures were homogenized by ball milling at 75 rpm (corresponding critical speed) for 24 hours and subsequently dried in a laboratory dryer at 105 °C for 24 hours. The chemical compositions of the raw materials were analyzed using X-ray fluorescence spectroscopy (XRF, Thermo Scientific Niton analyzer), while the crystalline phases were identified via X-ray diffraction (XRD, Rigaku D/Max III, 35 kV, 2θ range: 20–70). In addition, Differential Scanning Calorimetry (DSC, Netzsch) was employed to assess the thermal behavior of the materials.

The fly ash and porcelain powders contain significant amounts of Al_2O_3 and SiO_2 , with compositions as follows:

- ÇAT: 25.24 wt% Al₂O₃, 58.75 wt% SiO₂
- CAY: 13.11 wt% Al₂O₃, 50.98 wt% SiO₂
- KAN: 14.93 wt% Al₂O₃, 34.03 wt% SiO₂
- AFŞ: 4.63 wt% Al₂O₃, 9.37 wt% SiO₂
- Porcelain powder: 22.70 wt% Al₂O₃, 66.50 wt% SiO₂

Table 1. The chemical composition of fly ashes [62] and porcelain powder.

%	Porcelain	Fly Ashes				
	powder	ÇAT	ÇAY	KAN	AFŞ	
SiO ₂	66.50	58.75	50.98	34.03	9.37	
Al_2O_3	22.70	25.24	13.11	14.93	4.63	
TiO_2	0.10	-	-	-	-	
Fe_2O_3	0.30	5.76	9.74	4.41	2.58	
CaO	0.20	1.46	11.82	31.91	54.38	
MgO	0.10	2.22	3.91	1.73	1.54	
Na_2O	3.00	0.60	2.71	0.65	0.18	
K_2O	0.40	4.05	1.91	1.01	0.43	
SO_3	0.00	0.08	3.94	6.95	24.24	
LOI	6.70	1.12	0.86	3.60	2.8	

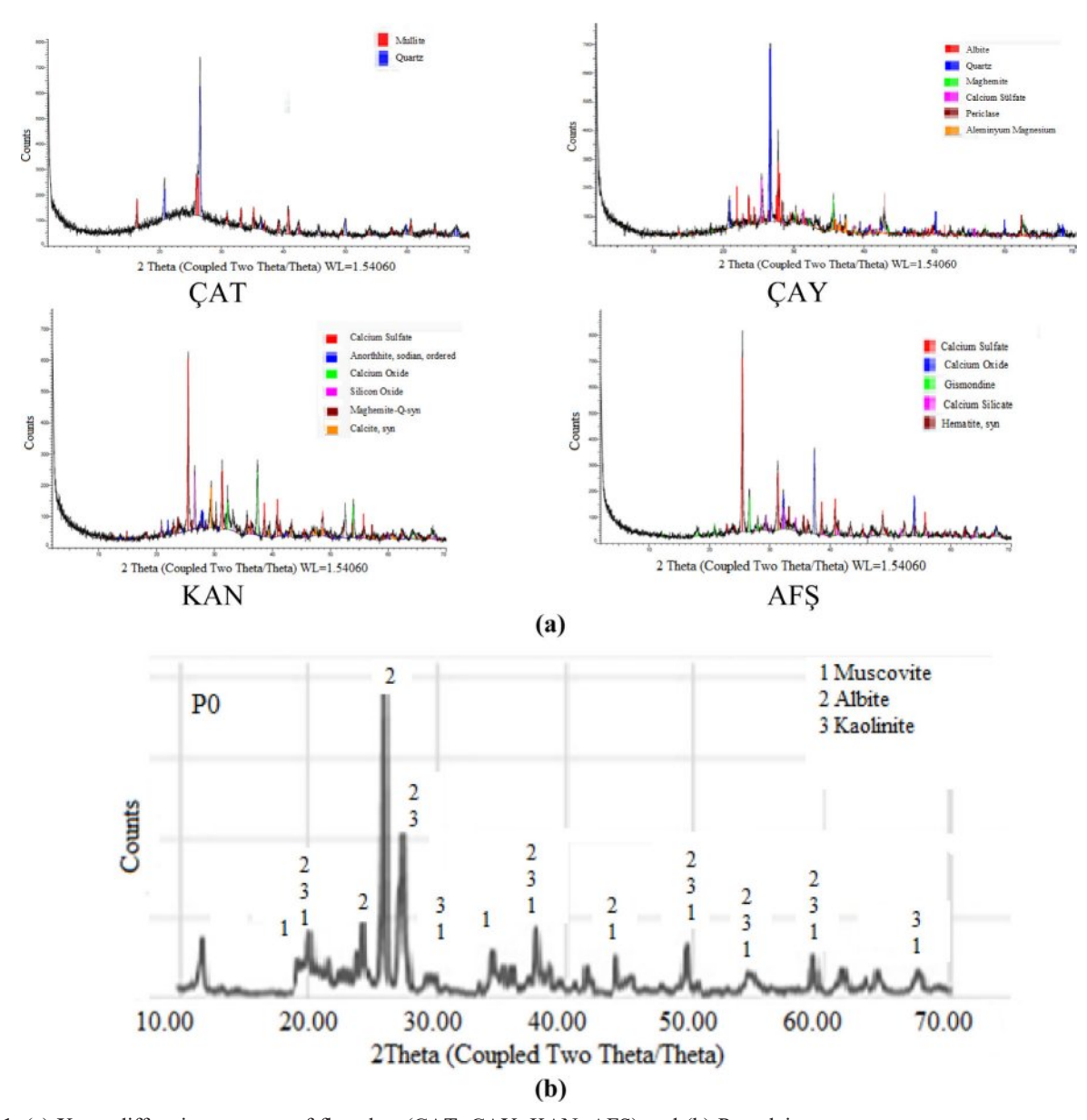


Fig. 1. (a) X-ray diffraction patterns of fly ashes (ÇAT, ÇAY, KAN, AFŞ) and (b) Porcelain masse.

These values are comparable to those of traditional ceramic raw materials.

X-ray diffraction (XRD) analysis of the porcelain body revealed the presence of silicon oxide, muscovite, calcium aluminosilicate, and iron silicate phases. The corresponding diffraction patterns are presented in Fig. 1(a–b). The XRD pattern of the Çatalağzı (ÇAT) fly ash (Fig. 1a) reveals prominent peaks corresponding to quartz (SiO₂) and mullite (Al₆Si₂O₁₃) [62]. In addition, a broad diffuse hump observed between 20° and 30° 20 indicates the presence of an amorphous glassy phase, which can enhance liquid-phase formation and facilitate densification during sintering. The Çayırhan (ÇAY) fly ash exhibits quartz as the dominant crystalline phase, accompanied by secondary phases such as albite (NaAlSi₃O₈), muscovite (KAl₂(AlSi₃O₁₀)(OH)₂), calcium sulfate, and other aluminosilicate minerals. The

presence of feldspathic phases (e.g., albite) may enhance vitrification behavior by acting as fluxing agents at elevated temperatures. The Kangal (KAN) fly ash is characterized by the presence of calcium silicate, calcium oxide, and sodium anorthite, indicating a higher CaO content. This composition suggests a propensity for early-stage liquidphase formation; however, excessive CaO may also induce structural inhomogeneities or phase separation at high concentrations. The Afsin-Elbistan A (AFS) fly ash displays a mineralogical composition dominated by anhydrite (CaSO₄), CaO, gismondine (a zeolitetype phase), and hematite (Fe₂O₃). The intense peaks associated with Ca- and sulfate-bearing phases indicate high reactivity and fluxing potential. Nonetheless, the elevated SO₃ content may promote excessive porosity or microcracking due to gas evolution during sintering. In contrast, the commercial porcelain powder (Fig. 1b)

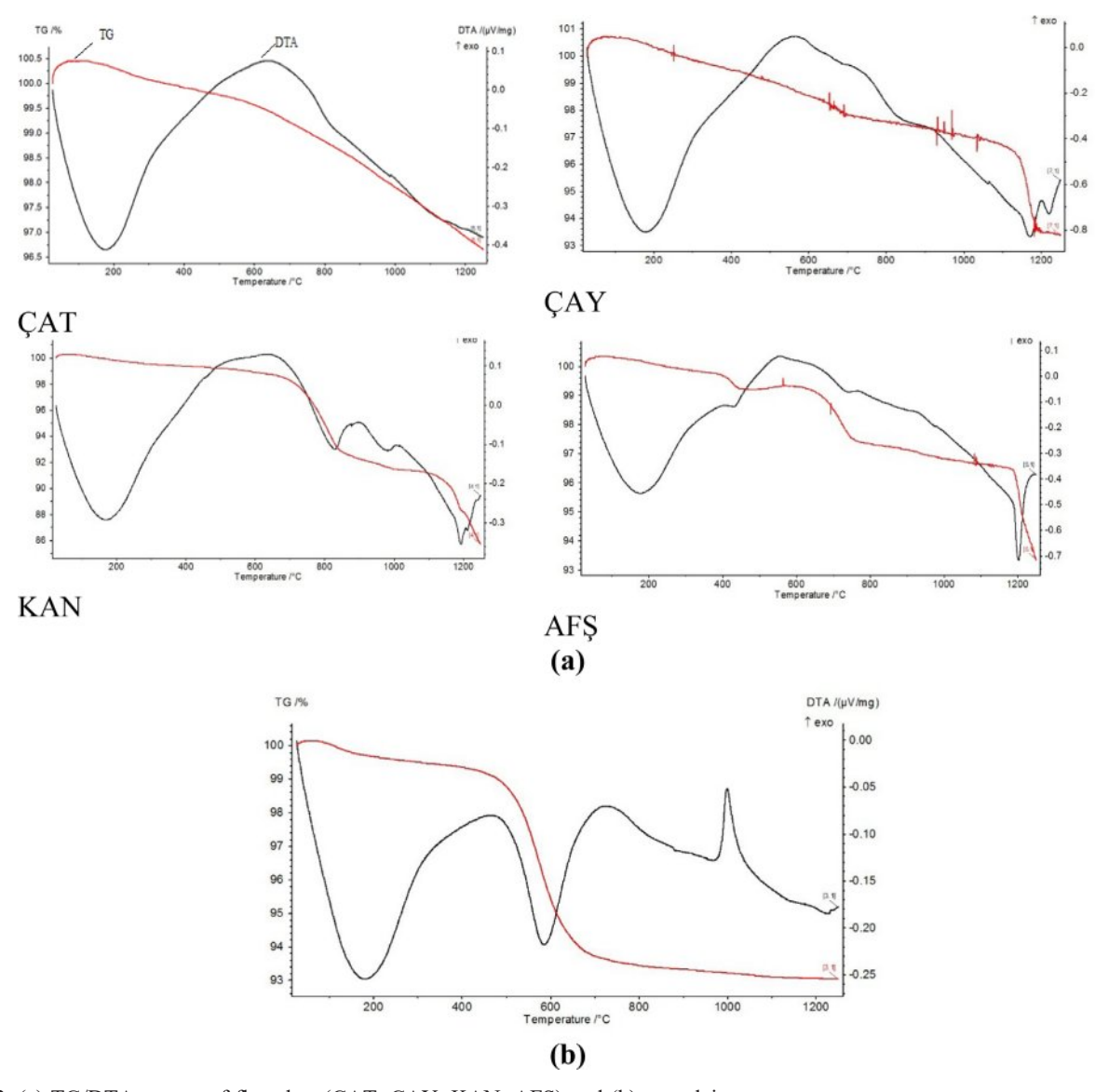


Fig. 2. (a) TG/DTA curves of fly ashes (ÇAT, ÇAY, KAN, AFŞ) and (b) porcelain masse

primarily contains albite, muscovite, and kaolinite as the main crystalline phases. Muscovite and albite function as fluxing agents and network modifiers, contributing to enhanced vitrification and densification during thermal processing.

The Differential Thermal Analysis/Thermogravimetric (DTA/TG) curves of the fly ash samples and the porcelain powder are presented in Fig. 2(a–b). The ÇAT fly ash (Fig. 2a) exhibited minimal total weight loss (~3%), consistent with its high-temperature combustion origin. The negligible mass loss observed between 25–400 °C confirms the absence of free or chemically bound water. An exothermic peak near 980 °C is attributed to mullite crystallization or the β -quartz to β -tridymite phase transition. The ÇAY fly ash demonstrated a total weight loss of approximately 7%, with thermal events occurring between 200–800 °C, likely due to the decomposition of residual hydrous minerals such as

muscovite. In contrast, the KAN fly ash displayed a more significant weight loss (~13–14%), primarily attributed to the decomposition of calcium-bearing phases and hydrated silicates, as evidenced by broad DTA peaks in the 800–1100 °C range. The AFŞ fly ash exhibited a similar weight loss (~7%), with distinct endothermic features likely corresponding to the decomposition of calcium sulfate near 600–800 °C. The DTA/TG curve of the porcelain powder (Fig. 2b) revealed a total weight loss of ~7%. The initial endothermic event occurring between 550–600 °C corresponds to the dehydroxylation of kaolinite to metakaolinite. A subsequent exothermic peak observed around 1000 °C is indicative of mullite formation, marking the onset of significant phase transformation.

Preparation of samples and characterization

All mixtures were stirred in distilled water for 24

hours at a rotational speed of 75 rpm. Fly ash was added to the porcelain bodies at concentrations of 0%, 15%, and 30% by weight to formulate the body compositions. Based on literature studies [39] and preliminary internal tests, the upper limit of fly ash content was set at 30 wt%. Additions beyond this threshold resulted in poor workability, increased cracking during drying, and deterioration of densification after sintering. Based on the results of the chemical analyses, an appropriate formulation was developed for porcelain compositions used in the ceramic industry. Samples were coded according to their composition and sintering temperature. For example, the code "P30ÇAT1150" refers to a porcelain sample containing 30% Çatalağzı fly ash and sintered at 1150 °C. The mixtures, homogenized in alumina ball mills, were shaped into bars of dimensions $20 \times 20 \times 100$ mm by uniaxial dry pressing at a pressure of 100 MPa. The green (unfired) samples were then sintered at temperatures of 1050 °C, 1100 °C, and 1150 °C for 1 hour. Although a fixed dwell time of 1 h was used in all sintering conditions to simulate industrial practice, it is acknowledged that longer durations could enhance mullite formation, particularly in high fly ash formulations [6]. Characterization of the sintered porcelain bodies included microstructural analysis (SEM), phase identification (XRD), mechanical testing (three-point bending), and physical property evaluation (shrinkage, water absorption, porosity, density, and color).

Linear shrinkage was measured using a digital caliper, and density, porosity, and water absorption were calculated based on Archimedes' principle, following ASTM C373-88 standards. Color analysis of the sintered samples was conducted using a Minolta CR-300 X-Rite colorimeter.

Mechanical strength was assessed using a three-point bending test on a mechanical testing device with a load sensitivity of 1 N and a capacity of 5 kN. For each sample, five measurements were taken, and the average was reported as the representative strength value. Phase composition was determined via X-ray diffraction (XRD) analysis over a 2θ range of 4°-70°, using a Panalytical X'Pert system, with phase identification carried out using the HighScore software. Prior to microstructural analysis, the samples were sequentially sanded using 400, 800, 1200, and 2000 grit abrasive papers, followed by polishing with a 1 µm diamond suspension on a velvet cloth. Scanning Electron Microscopy (SEM) and Energy Dispersive Spectroscopy (EDS) analyses were performed using a Mira3 XMU FE-SEM (Tescan, Czech Republic). All experimental data were compiled into graphs and tables for interpretation and discussion.

The sintered samples underwent the following analyses: physical tests (including total shrinkage, porosity, density, water absorption, and color), mechanical testing (three-point bending), microstructural analysis using Scanning Electron Microscopy (SEM), and Energy Dispersive X-ray Spectroscopy (EDX), and phase analysis using X-ray Diffraction (XRD). All measurements and calculations were performed in 3 to 5 replicates, and arithmetic mean values were used for data evaluation.

Results and Discussion

The results of physical property measurements—including water absorption (WA), porosity, bulk density, and total shrinkage—are summarized in Table 2 and illustrated in Fig. 3(a–b-c) and Fig. 4(a–b-c). In general, increasing the

Table 2. Water absorption	 porosity, bulk densi 	ty and total shrinkage	tests of porcelain samples.

Sample	Water absorption (%)	Porosity (%)	Bulk density (g/cm³)	Total Shrinkage %
P00ÇAT1050	14.284	27.260	1.910	2.46
P15ÇAT1050	15.681	28.441	1.814	2.48
P30ÇAT1050	15.876	30.226	1.909	2.74
P00ÇAT1100	8.811	18.398	2.088	6.29
P15ÇAT1100	7.515	15.665	2.085	6.17
P30ÇAT1100	8.150	16.515	2.026	6.56
P00ÇAT1150	3.213	7.274	2.273	8.98
P15ÇAT1150	1.829	4.197	2.295	9.25
P30ÇAT1150	1.034	2.366	2.289	9.79
P00ÇAY1050	14.284	27.260	1.910	2.46
P15ÇAY1050	15.670	28.867	1.845	2.08
P30ÇAY1050	17.440	31.128	1.785	1.42
P00ÇAY1100	8.811	18.398	2.088	6.29
P15ÇAY1100	11.966	22.891	1.936	4.32
P30ÇAY1100	14.810	27.010	1.825	2.55
P00ÇAY1150	3.213	7.274	2.273	8.98
P15ÇAY1150	1.660	3.683	2.219	7.39
P30ÇAY1150	2.391	4.948	2.082	5.65

Table 2. Continued

Sample	Water absorption (%)	Porosity (%)	Bulk density (g/cm³)	Total Shrinkage %
P00KAN1050	14.284	27.260	1.910	2.46
P15KAN1050	19.649	33.739	1.718	1.35
P30KAN1050	24.728	39.009	1.579	0.74
P00KAN1100	8.811	18.398	2.088	6.29
P15KAN1100	18.353	31.888	1.738	1.99
P30KAN1100	22.129	36.097	1.632	1.23
P00KAN1150	3.213	7.274	2.273	8.98
P15KAN1150	10.443	19.515	1.871	4.28
P30KAN1150	15.037	25.902	1.724	2.65
P00AFŞ1050	14.284	27.260	1.910	2.46
P15AFŞ1050	18.897	33.068	1.750	1.31
P30AFŞ1050	22.905	37.502	1.640	0.51
P00AF\$1100	8.811	18.398	2.088	6.29
P15AFŞ1100	16.196	29.276	1.808	2.04
P30AF\$1100	19.638	33.470	1.712	1.33
P00AFŞ1150	3.213	7.274	2.273	8.98
P15AFŞ1150	11.658	21.594	1.853	3.29
P30AFŞ1150	16.466	28.238	1.717	2.38

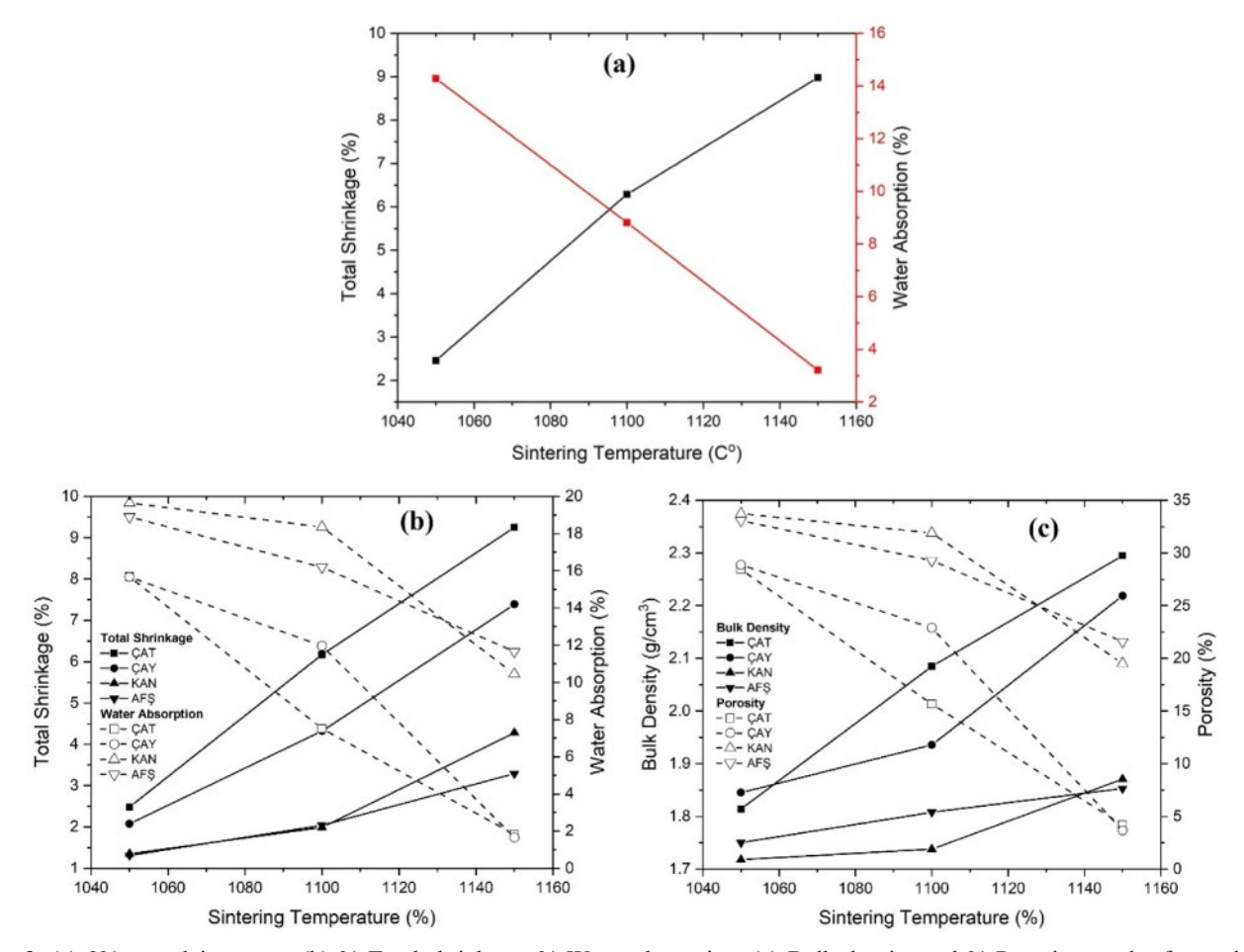


Fig. 3. (a) 0% porcelain masse, (b) % Total shrinkage, % Water absorption, (c) Bulk density and % Porosity graph of porcelain samples %15 fly ash.

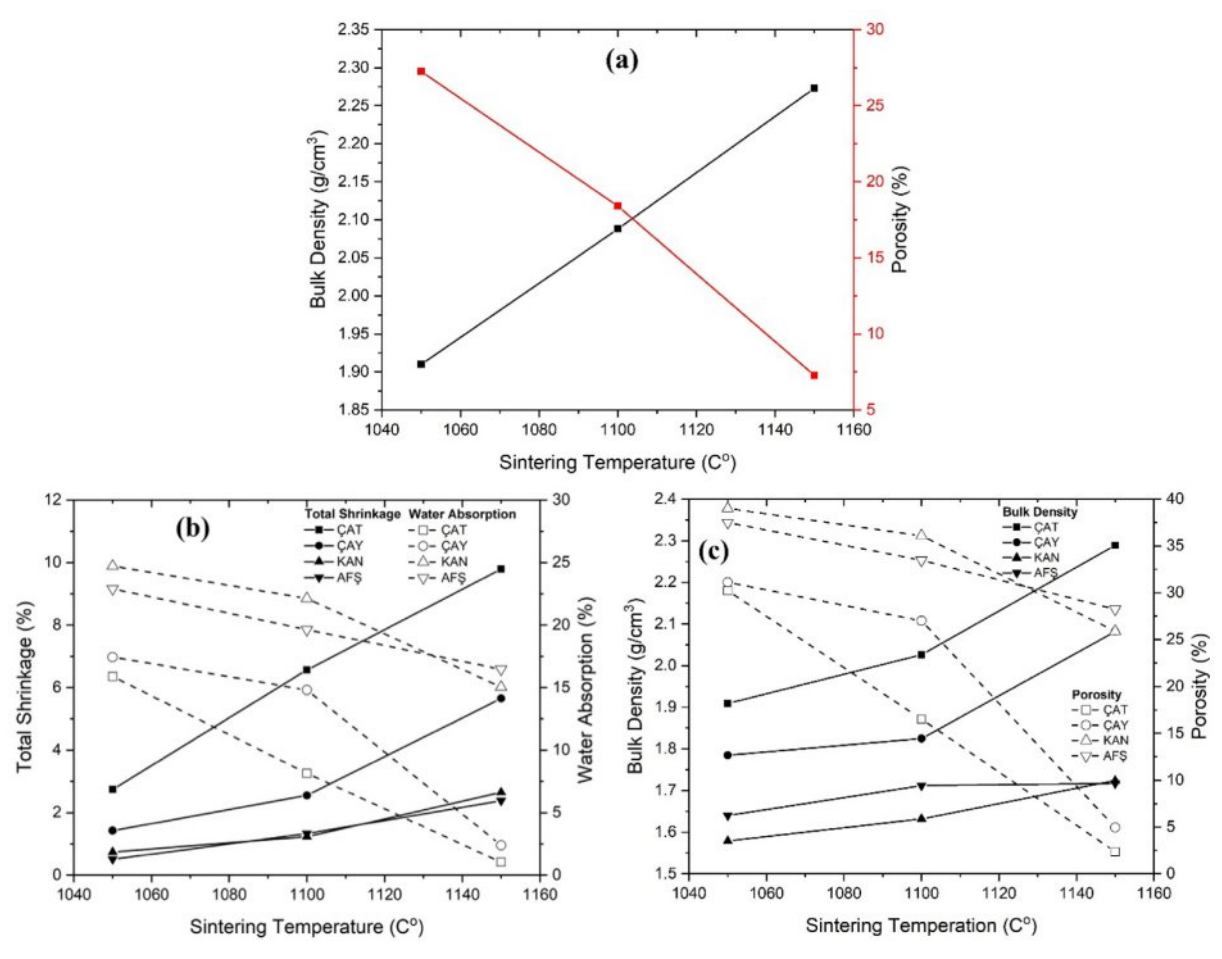


Fig. 4. (a) 0% porcelain masse, (b) % Total shrinkage and % Water absorption, (c) Bulk density and % Porosity graph of porcelain samples %30 fly ash.

sintering temperature led to improved densification, as indicated by reductions in porosity and water absorption, and corresponding increases in bulk density and total shrinkage. For all compositions, the highest porosity and WA values were observed at 1050 °C, while firing at 1150 °C promoted enhanced densification. The effect of fly ash incorporation, however, was more nuanced and strongly influenced by the source material. Notably, ÇAT fly ash significantly enhanced densification at 1150 °C: water absorption decreased from 3.21% (0 wt% fly ash) to 1.03% (30 wt% fly ash), and bulk density increased to 2.289 g/cm³. In contrast, samples containing AFŞ and KAN fly ashes exhibited consistently higher porosity and water absorption across all firing temperatures, suggesting incomplete vitrification—likely due to the elevated CaO and SO3 contents in these ashes, which can promote excessive liquid-phase formation and gas evolution. Interestingly, at 1050 °C, increasing the fly ash content generally resulted in elevated porosity and water absorption for CAY, KAN, and AFS samples, potentially due to their lower amorphous phase content and higher volatile release during early-stage sintering. Nevertheless, at 1150 °C, certain fly ash-containing compositions—particularly those incorporating CAT and ÇAY ashes—demonstrated markedly improved physical properties compared to the control, indicating the importance of both firing temperature and ash chemistry in governing densification behavior.

The irregular trend in water absorption may be linked to fly ash particle agglomeration or heterogeneity in its dispersion within the matrix. Such effects become more pronounced at higher concentrations, potentially hindering homogeneous vitrification and promoting residual porosity [48,49].

Color analysis of the sintered porcelain samples was performed, and the results are presented in Table 3. The L value indicates lightness (ranging from 0 = black to 100 = white), while +a and +b represent the red and yellow components, respectively. In the unreinforced porcelain samples (P00), increasing the sintering temperature resulted in a moderate reduction in L values, likely due to intensified phase transformation and densification. Nevertheless, the surfaces remained relatively white, with the highest lightness (L = 90.58) observed in the P00 sample fired at 1050 °C. The incorporation of fly ash led to a marked decrease in lightness and a corresponding increase in chromaticity (+a, +b), an effect that became more pronounced with

Table 3. Colour analysis of porcelain sintered samples.

	1						
Samples	L	a	b	Samples	L	a	b
P00ÇAT1050	90.58	2.64	5.91	P00KAN1050	90.58	2.64	5.91
P15ÇAT1050	84.32	4.71	10.01	P15KAN1050	84.28	4.56	7.76
P30ÇAT1050	79.13	6.99	14.45	P30KAN1050	80.96	5.19	10.06
P00ÇAT1100	88.63	2.34	7.89	P00KAN1100	88.63	2.34	7.89
P15ÇAT1100	74.74	7.87	14.90	P15KAN1100	84.15	3.32	9.25
P30ÇAT1100	68.73	10.23	18.62	P30KAN1100	81.52	3.25	12.83
P00ÇAT1150	83.25	1.87	10.54	P00KAN1150	83.25	1.87	10.54
P15ÇAT1150	63.56	3.94	11.00	P15KAN1150	70.09	6.41	17.95
P30ÇAT1150	55.19	4.69	11.76	P30KAN1150	69.02	5.83	22.66
P00ÇAY1050	90.58	2.64	5.91	P00AFŞ1050	90.58	2.64	5.91
P15ÇAY1050	79.67	5.51	8.86	P15AFŞ1050	84.97	3.67	7.08
P30ÇAY1050	74.93	6.48	10.43	P30AF\$1050	79.47	4.53	8.38
P00ÇAY1100	88.63	2.34	7.89	P00AF\$1100	88.63	2.34	7.89
P15ÇAY1100	75.89	5.48	9.69	P15AFŞ1100	83.43	2.98	8.97
P30ÇAY1100	69.20	6.77	11.09	P30AFŞ1100	79.75	3.13	10.98
P00ÇAY1150	83.25	1.87	10.54	P00AF\$1150	83.25	1.87	10.54
P15ÇAY1150	57.13	3.63	10.57	P15AFŞ1150	74.64	4.83	14.90
P30ÇAY1150	43.30	4.49	9.96	P30AFŞ1150	66.27	6.98	24.63

higher firing temperatures and greater additive content. For instance, in the P30ÇAY1150 sample, L sharply declined to 43.30, while a and b increased to 4.49 and 9.96, respectively. These color changes are primarily attributed to the presence of Fe₂O₃, TiO₂, and alkali oxides in the fly ash, which promote the formation of color-imparting phases such as hematite, fayalite, or colored amorphous glass during sintering. Interestingly, despite its relatively high Fe₂O₃ content, the ÇAT fly ash yielded better color stability—possibly due to its lower alkali content and greater mullite formation, which may suppress discoloration by limiting the formation of colored secondary phases.

The three-point bending strength values of the porcelain samples are summarized in Table 4 and illustrated in Fig. 5. Overall, increasing the sintering temperature

Table 4. Three-point bending strength of samples (MPa).

	*			` ′		
Commlas	3-point bending strength (MPa)					
Samples	ÇAT	ÇAY	KAN	AFŞ		
P001050	6.764	6.764	6.764	6.764		
P151050	6.064	7.249	4.975	4.796		
P301050	6.447	5.188	4.691	4.853		
P001100	12.181	12.181	12.181	12.181		
P151100	12.812	9.312	4.600	7.868		
P301100	13.510	5.371	4.207	5.274		
P001150	16.255	16.255	16.255	16.255		
P151150	20.585	17.847	8.731	9.984		
P301150	20.149	15.280	7.252	7.822		

significantly enhanced the mechanical strength, consistent with improved densification and phase development at elevated temperatures. However, the effect of fly ash addition varied substantially depending on the source material. Among the fly ashes investigated, CAT fly ash demonstrated the most pronounced strengthening effect: the flexural strength increased from 16.26 MPa (P00) to 20.58 MPa (P15) at 1150 °C. This improvement is attributed to the high SiO2 and Al2O3 contents, as well as the presence of mullite precursors in the CAT ash, which contributed to the formation of a denser microstructure. In contrast, samples incorporating KAN and AFS fly ashes exhibited a decline in mechanical performance with increasing additive content, particularly at 1100-1150 °C. The elevated levels of CaO and SO₃ in these ashes likely led to excessive liquid phase formation and gas release during sintering, promoting residual porosity and reducing flexural strength. The CAY fly ash, which is moderately rich in iron and alkali oxides, still improved strength at 15 wt% addition (17.85 MPa at 1150 °C); however, mechanical performance declined at 30 wt%, indicating an optimal additive threshold below 20 wt%. Although the 30 wt.% fly ash sample still exhibited higher strength than the reference (0%), its value was slightly lower than the 15 wt.% sample. This suggests an optimum threshold near 15 wt.%, beyond which excessive ash content impairs vitrification and leads to local structural inhomogeneity.

X-ray diffraction (XRD) patterns of the control (P0) and porcelain samples incorporating 30 wt% fly ashes, fired at 1050 °C and 1150 °C, are presented in Fig. 6

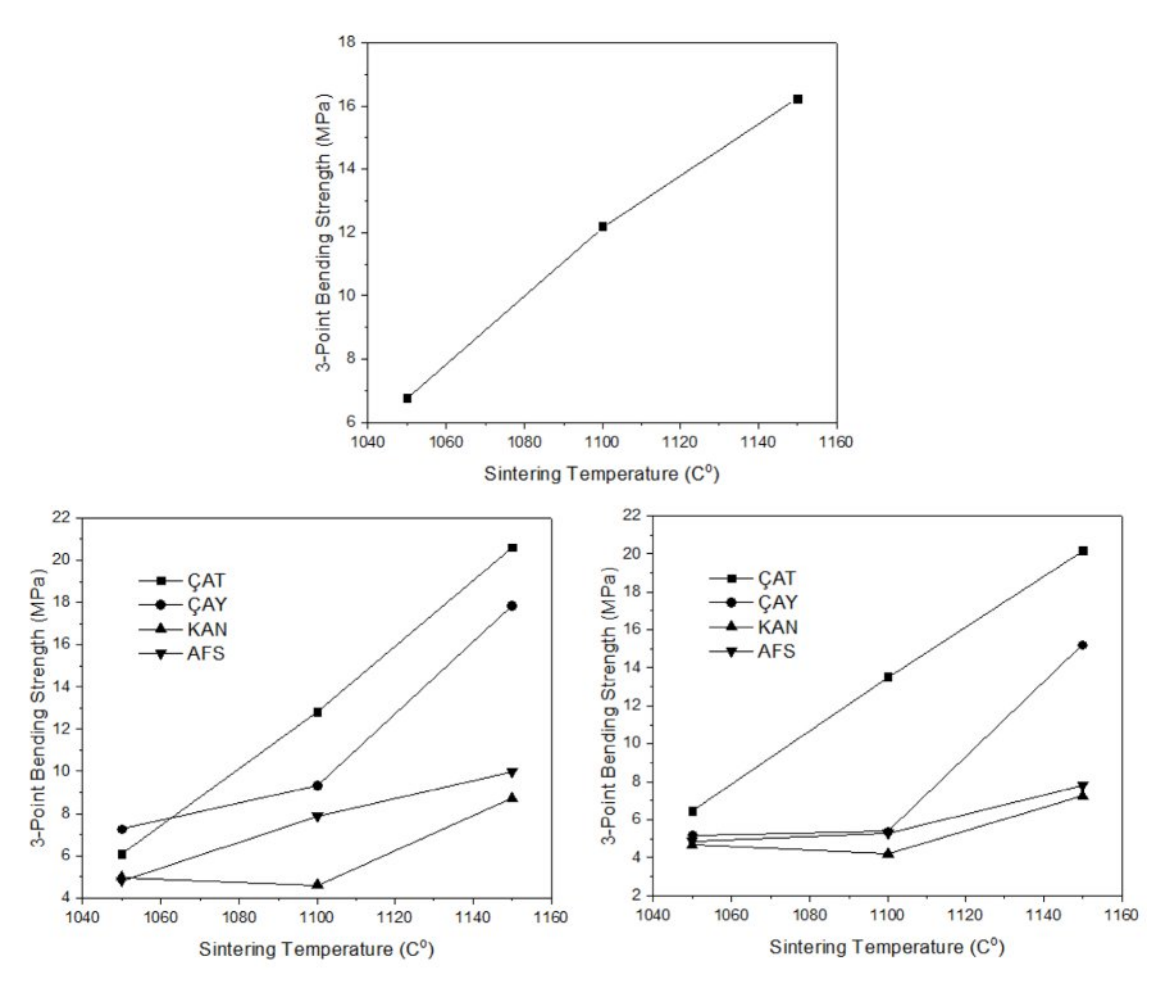


Fig. 5. 3-point bending strength graph of porcelain samples (a-0% porcelain masse, b-15% fly ash, c-30% fly ash).

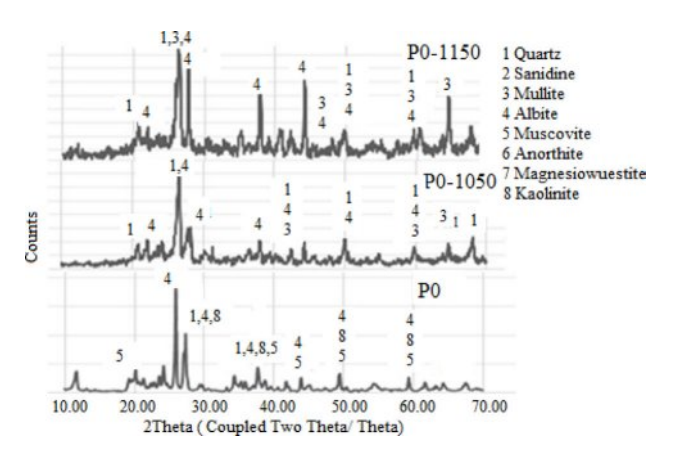


Fig. 6. XRD patterns of porcelain samples (P0, P0-1050 and P0-1150).

and Fig. 7. The starting porcelain powder (P0) primarily comprises quartz (JCPDS 96-900-9667), albite (96-900-1632), kaolinite (96-101-1046), and muscovite (96-101-1050). Upon firing at 1050 °C, the emergence of mullite (96-900-5502) suggests the initiation of phase transformation, predominantly from the decomposition of kaolinite. As the temperature increases to 1150 °C, the peaks associated with kaolinite and muscovite disappear,

while the mullite peaks become more prominent, indicating enhanced crystallization and densification. Among the fly ash-added compositions, P30CAT1150 exhibited the most pronounced mullite peak intensity, which can be attributed to the high alumina and silica content of the ÇAT fly ash. This result suggests effective mullitization, potentially contributing to improved mechanical performance. In contrast, P30KAN1150 and P30AF\$1150 samples displayed comparatively weaker mullite signals and a predominance of quartz and anorthite phases, implying limited mullite formation. This behavior may be related to the elevated CaO and SO₃ contents in these fly ashes, which likely promote the formation of a low-viscosity glassy phase that inhibits mullite crystallization. Overall, the XRD results confirm that the type of fly ash significantly influences crystalline phase evolution and, consequently, the final properties of the porcelain bodies.

Scanning electron microscopy (SEM) images of the non-additive porcelain samples (P0), sintered at 1050 °C and 1150 °C, are presented in Fig. 8. At 1050 °C, the microstructure appears relatively porous and heterogeneous, characterized by large glassy-phase regions and unreacted quartz grains. This morphology reflects incomplete densification and limited mullite

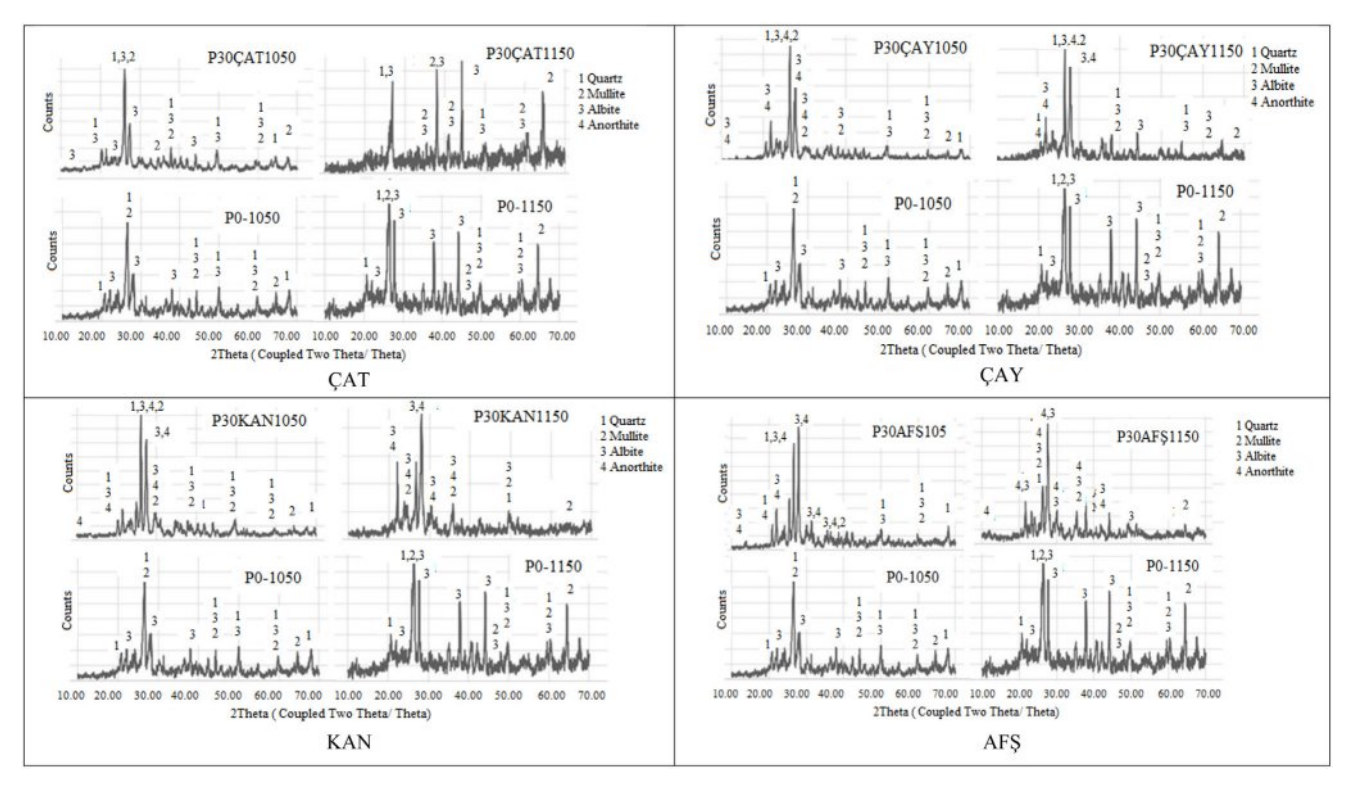


Fig. 7. XRD pattern of 30% wt. fly ashes (ÇAT, ÇAY, KAN, AFŞ) additive porcelain samples sintered 1050 °C and 1150 °C.

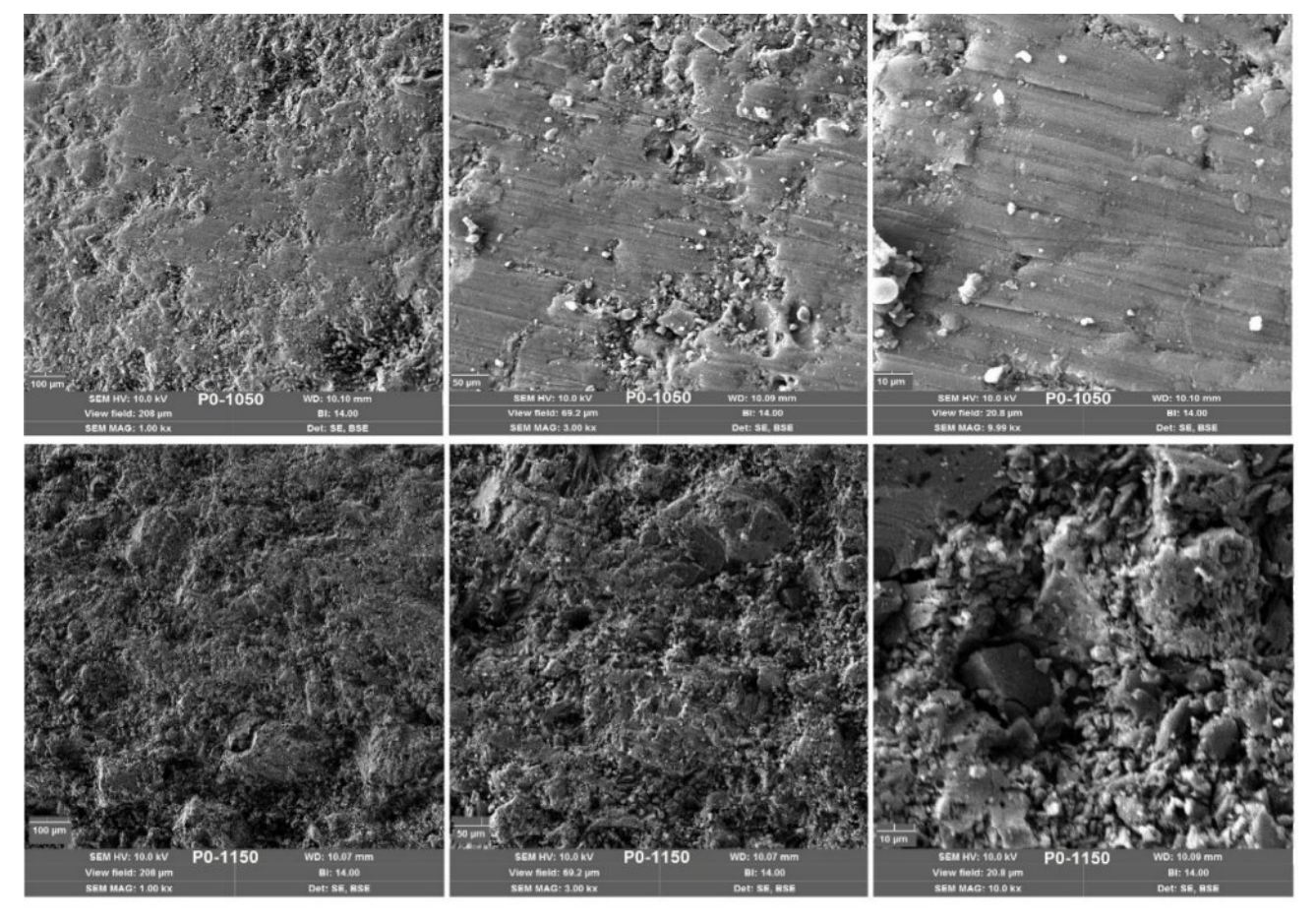


Fig. 8. SEM images of non-additive porcelain samples.

formation, indicating that the sintering process at this temperature was insufficient to achieve full vitrification. In contrast, at 1150 °C, the microstructure becomes noticeably denser and more vitrified. The emergence of needle-like mullite crystals embedded within the continuous glassy matrix is indicative of the onset of mullitization and advanced phase transformation. These microstructural features correlate well with the observed improvements in mechanical strength and water resistance at this temperature. Overall, the increase in sintering temperature promotes enhanced densification, phase development, and microstructural integrity, consistent with the findings from XRD analysis and physical property measurements.

Energy Dispersive Spectroscopy (EDS) analysis of the reference porcelain sample sintered at 1050 °C (P0-1050) is presented in Fig. 9. The results reveal a dominant presence of SiO₂ (57.94 wt%) and Al₂O₃ (25.85 wt%), characteristic of aluminosilicate-rich porcelain compositions. These oxides primarily originate from quartz, kaolinite, and mullite precursors. Significant levels of Na₂O (8.97 wt%) and K₂O (2.64 wt%) were also detected, indicating the presence of feldspathic phases such as albite and muscovite, which act as fluxing agents and facilitate the formation of a glassy phase during sintering. Minor components include Fe₂O₃ (3.19 wt%) and CaO (1.19 wt%). While the relatively low CaO content is advantageous in reducing vitrification-

ST STATE OF THE ST	P0010	50			1
	0	58.97	Na ₂ O	8.97	1
	Na	2.82	MgO	0.22	1
	Mg	0.11	Al ₂ O ₃	25.85	1
	Al	11.60	SiO ₂	57.94	1
TO ME	Si	22.96	K ₂ O	2.64	1
	K	0.93	CaO	1.19	
2003	Ca	0.72	TiO ₂	0.00	1
	Ti	0.00	Fe ₂ O ₃	3.19	
6	Fe	1.89			1
Electron Image 1	P0011	50			_
\$ - \$ · · ·	О	64.79	Na ₂ O	12.50	
A	Na	3.44	MgO	0.00	
* ** C 7	Mg	0.00	Al ₂ O ₃	26.54	
	Al	10.42	SiO ₂	56.52	
10 July 10 10 10 10 10 10 10 10 10 10 10 10 10	Si	19.60	K ₂ O	2.73	
	K	0.84	CaO	1.72	
	Ca	0.91	TiO ₂	0.00	
W	Ti	0.00	Fe ₂ O ₃	0.00	
	Fe	0.00			

Fig. 9. SEM-EDS images of non-additive porcelain samples.

related defects (e.g., excessive liquid phase or bloating), the iron content may contribute to subtle coloration at elevated temperatures through the formation of ironbearing phases.

The Energy Dispersive Spectroscopy (EDS) spectrum of the reference porcelain sample sintered at 1150 °C (P0-1150) is shown in Fig. 9. Compared to the sample

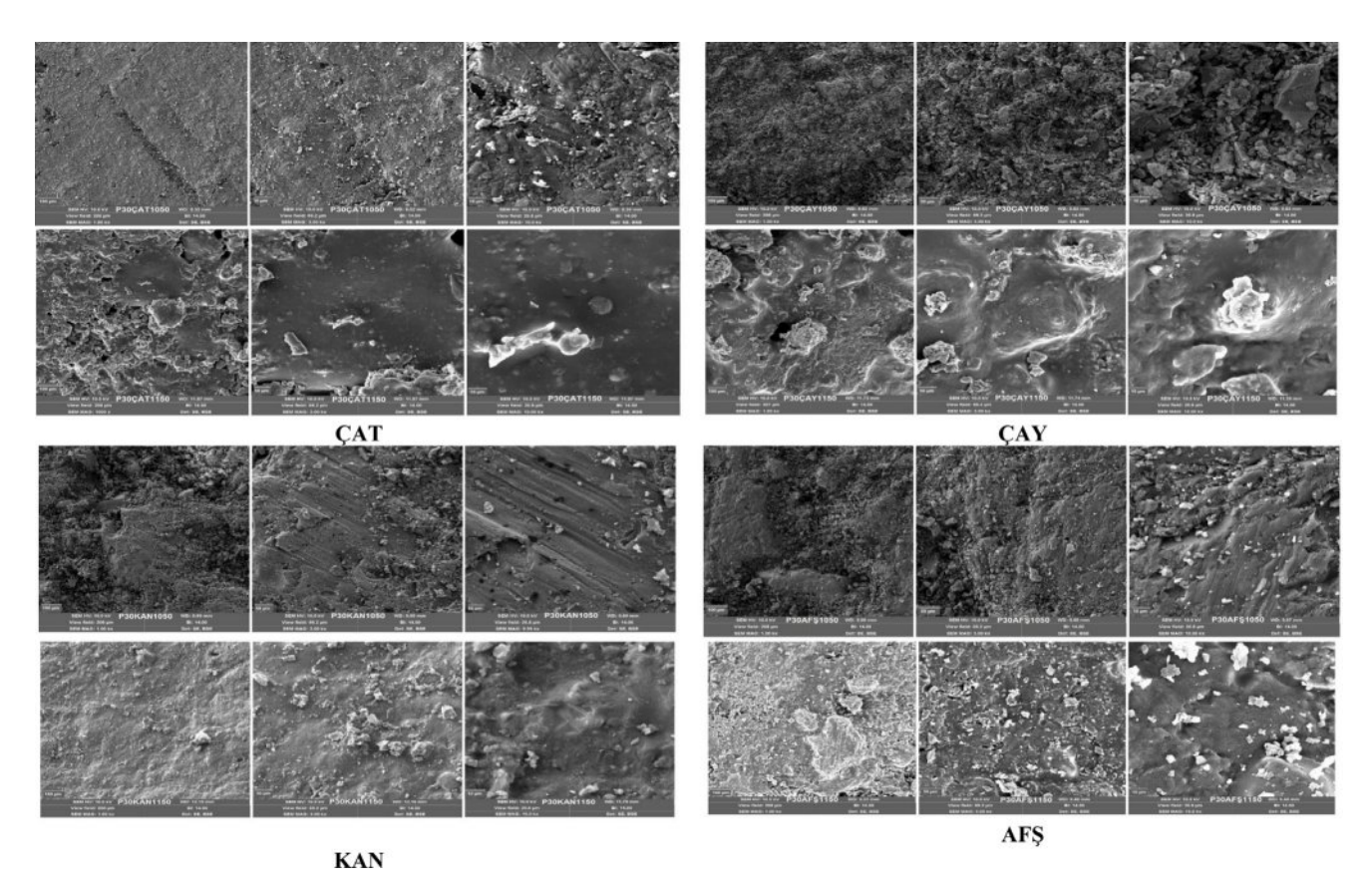


Fig. 10. SEM images of 30% fly ashes (ÇAT, ÇAY, KAN, AFŞ) added porcelain samples sintered at 1050 °C and 1150 °C.

sintered at 1050 °C, the 1150 °C specimen exhibits a notably higher Na₂O content (12.50 wt%), suggesting increased formation of a glassy phase derived from albite at elevated temperatures. The concentrations of Al₂O₃ (26.54 wt%) and SiO₂ (56.52 wt%) remain consistently high, aligning with the expected presence of mullite and residual quartz. Notably, Fe₂O₃ and TiO₂ were not detected, indicating a purer ceramic matrix, which is advantageous for achieving high whiteness and minimizing discoloration in the fired product. The increase in sintering temperature promotes enhanced vitrification, phase development, and microstructural densification, as corroborated by the SEM results and the oxide composition identified in the EDS analysis.

SEM micrographs of porcelain samples incorporating 30 wt% fly ash from different sources (ÇAT, ÇAY, KAN, and AFŞ), sintered at 1050 °C and 1150 °C, are presented in Fig. 10. Among the compositions, the P30ÇAT1150 sample exhibits the highest degree of densification and microstructural homogeneity, characterized by the presence of needle-like mullite crystals embedded within a continuous glassy matrix. This refined morphology is consistent with the improved physical and mechanical performance observed for ÇAT-derived samples. In contrast, the P30ÇAY and P30AFŞ samples retain

relatively high porosity and display incomplete fusion of heterogeneous particles, even at 1150 °C. These features are likely attributable to the high CaO and low SiO₂ contents of ÇAY and AFŞ fly ashes, which can disrupt mullite formation and hinder vitrification. The P30KAN specimens demonstrated the poorest microstructural integrity, exhibiting widespread porosity, microcracking, and limited evidence of phase development. The high calcium content and low amorphous fraction of KAN fly ash may contribute to these deficiencies. Overall, the microstructural evolution supports the conclusion that fly ash sourced from the Çatalağzı (ÇAT) power plant exhibits the highest compatibility with porcelain matrices, effectively promoting densification and mullite crystallization during sintering.

The elemental compositions of the porcelain samples containing 30 wt% fly ash (P30), sintered at 1050 °C and 1150 °C, as determined by Energy Dispersive Spectroscopy (EDS) in Fig. 11 according to the general regional results (♣), exhibit significant variations depending on the fly ash source. The P30ÇAT1150 sample demonstrated the most favourable chemical profile, with the highest SiO₂ content (63.93 wt%), elevated Na₂O (6.71 wt%), and the complete absence of Fe₂O₃. This composition supports the formation of a

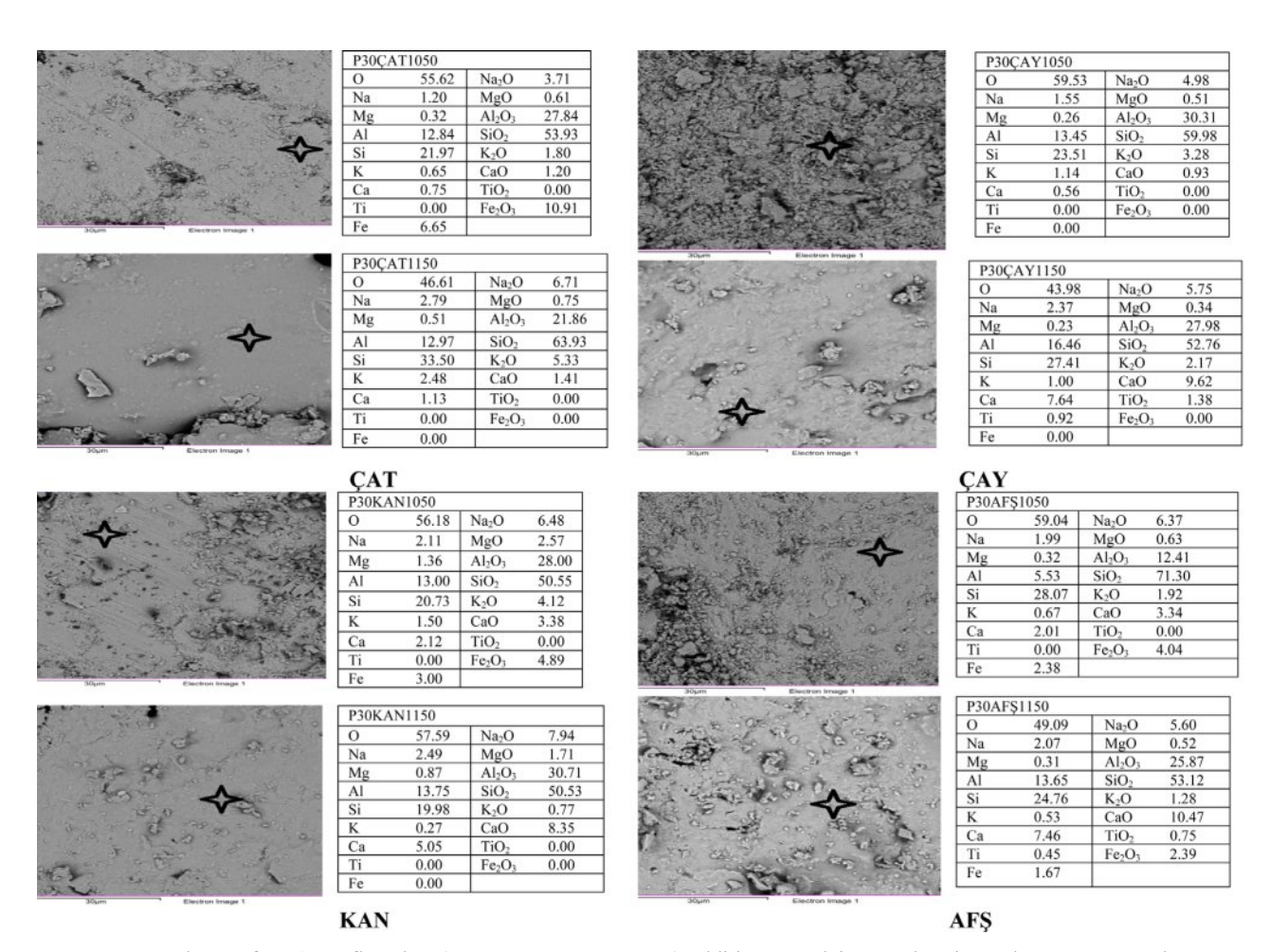


Fig. 11. EDS analyses of 30% wt. fly ashes (ÇAT, ÇAY, KAN, AFŞ) additive porcelain samples sintered at 1050 °C and 1150 °C.

homogeneous glassy matrix, contributing to enhanced vitrification and improved mechanical performance. By contrast, the P30CAY1150 and P30AF\$1150 samples exhibited high CaO concentrations (9.62 wt% and 10.47 wt%, respectively), which are known to disrupt mullite crystallization and interfere with vitrification, potentially leading to increased porosity and microstructural defects. Although the P30KAN1150 specimen displayed an elevated Al₂O₃ content (30.71 wt%), its comparatively low SiO2 and insufficient alkali content may have restricted densification and phase development during sintering. These compositional differences are in strong agreement with the corresponding physical, mechanical, and microstructural findings, reinforcing that Çatalağzı (CAT) fly ash is the most compatible additive for enhancing porcelain sintering behavior and final material performance.

Conclusions

This study systematically evaluated the effects of fly ash sourced from four thermal power plants—Çatalağzı (ÇAT), Çayırhan (ÇAY), Kangal (KAN), and Afşin–Elbistan A (AFŞ)—on the physicochemical, microstructural, and mechanical properties of porcelain ceramics. Fly ash was incorporated into a commercial porcelain matrix at 15 wt% and 30 wt%, followed by sintering at 1050–1150 °C. The findings revealed significant differences in densification behavior and final performance, largely dictated by the chemical composition of the respective fly ashes.

- Among all compositions, the ÇAT-derived fly ash demonstrated the most favorable performance. Its high SiO₂/Al₂O₃ ratio and the absence of Fe₂O₃ in the sintered matrix facilitated the development of a dense microstructure, as confirmed by SEM and EDS analyses, and promoted the formation of needle-like mullite crystals, as evidenced by XRD patterns. These features translated into the lowest porosity (2.366%) and water absorption (1.034%), along with the highest flexural strength (20.585 MPa) at 1150 °C, indicating efficient vitrification and mechanical reinforcement.
- As the sintering temperature increased, the whiteness (L) value of the porcelain samples decreased, while the yellowish tone (b) value increased. These changes are primarily attributed to the presence of fluxing oxide impurities and potential Fe₂O₃-related chromophores originating from the fly ash.
- The compressive strength of the porcelain samples generally improved with higher sintering temperatures. The strength value of the pure porcelain sample sintered at 1150 °C was 16.255 MPa. In comparison, the sample containing 15% Çatalağzı fly ash, sintered at the same temperature, reached a strength of 20.585 MPa, while the sample with 30% fly ash achieved 20.149 MPa. In contrast, samples

- containing KAN and AFŞ fly ashes exhibited inferior densification, higher residual porosity, and reduced mechanical strength. These shortcomings are attributed to their excessive CaO content and poor phase compatibility with the porcelain matrix. Furthermore, DSC/TG analysis revealed a distinct exothermic peak near 980 °C in the ÇAT sample, corresponding to mullite crystallization, while AFŞ and KAN samples exhibited multiple thermal events associated with complex decomposition and limited ceramic reactivity.
- SEM analysis revealed that microstructural porosity decreased as the firing temperature increased, due to the development of a liquid phase. Porosity was more evident at lower temperatures. Moreover, the formation of mullite at higher temperatures contributed to improved strength. The limited amount and fine size of quartz grains observed in the SEM images also positively influenced the mechanical strength.

In conclusion, this study demonstrates that the incorporation of fly ash—traditionally considered a waste product—into porcelain formulations, in controlled amounts, can lead to the production of high-strength porcelain. This not only offers an environmentally friendly solution for fly ash disposal but also helps conserve natural raw material resources, contributing to sustainable ceramic production. Çatalağzı fly ash, in particular, emerges as a promising sustainable raw material for porcelain production by supporting the valorization of industrial by-products in advanced ceramic manufacturing.

Acknowledgements

The authors wish to acknowledge the Scientific Research Projects Coordination Unit (CÜBAP-Project No:M-698) the facility and support extended for the research work.

References

- W.M. Carty and U. Senapati, J. Am. Ceram. Soc. 81[1] (1998) 3-20.
- Y. Iqbal and W.E. Lee, J. Am. Ceram. Soc. 82[12] (1999) 3584-3590.
- 3. F.H. Norton, "Fine Ceramics: Technology and Applications", (2nd ed., Robert E. Krieger Publishing Company Inc., FL. 1978) p.507.
- W.D. Kingery, H.K. Bowen, and D.R. Ulhmann, "Introduction to Ceramics" (Wiley and Sons New York, 1976) p.177-216.
- 5. T. Tarvornpanich, G.P. Souza, and W.E. Lee, J. Am. Ceram. Soc. 88[5] (2005) 1302-1308.
- J. Martín-Márquez, A.G. De la Torre, M.A. Aranda, J.M. Rincón, and M. Romero, J. Am. Ceram. Soc. 92[1] (2009) 229-234.
- D.I. Seymour, M.S Thesis (New York State College of Ceramics at Alfred University Alfred NY 2000).

- W. Lerdprom, M.S Thesis (New York State College of Ceramics at Alfred University Alfred NY 2014).
- H. Lee and W.M. Carty, in Proceedings of the 106th Annual Meeting and Exposition of the Am. Cer. Soc. 2004 p.18.
- W.M. Carty, In Ceram. Eng. and Sci. Proceed., Columbus, Ohio, Am. Ceram. Soci. 23[2] (2002) 79-94.
- B. Pinto, W. Carty, and S. Misture, in Science of Whiteware, III, (Alfred University 2000).
- E. Rambaldi, W.M. Carty, A. Tucci, and L. Esposito, Ceram. Inter. 33[5] (2007) 727-733.
- A. Shah, M.S. Thesis (New York State College of Ceramics at Alfred University Alfred NY 2007).
- S.G.D. Iya, M.Z. Noh, S.N. Ab Razak, N. Sharip, and N.A.A. Kutty, Inter. J. Nanoelectronics Mater. 12[2] (2019).
- D. Gouvêa, T.T. Kaneko, H. Kahn, E. de Souza Conceição, and J.L. Antoniassi, Ceram. Inter. 41[1] (2015) 487-496.
- Z. Xian, L. Zeng, X. Cheng, and H. Wang, J. Therm. Analysis and Calorimetry 122[2] (2015) 997-1004.
- M. Tarhan, B. Tarhan, and T. Aydin, Ceram. Inter. 42[15] (2016) 17110-17115.
- 18. A. Shui, X. Xi, Y. Wang, and X. Cheng, Ceram. Inter. 37[5] (2011) 1557-1562.
- J.C. Hower, C.L. Senior, E.M. Suuberg, R.H. Hurt, J.L. Wilcox, and E.S. Olson, Prog. Energy and Combust. Sci. 36[4] (2010) 510-529.
- S. Singh, L.C. Ram, R.E. Masto, and S.K. Verma, Int. J. Coal Geol. 87[2] (2011) 112-120.
- H.B. Vuthaluru and D. French, Fuel Process. Technol. 89[6] (2008) 595-607.
- 22. Surabhi, Intern. J. Appl. Chem. 13[1] (2017) 29-52.
- 23. Z. Çetinkaya, J. Faculty of Eng. and Arch. Gazi University 37[1] (2022) 137-144.
- N.S. Fishman, C.A. Rice, G.N. Breit, and R.D. Johnson, Fuel 78[2] (1999) 187-196.
- S. Adjei and S. Elkatatny, J. Petrol. Sci. Eng. 195 (2020) 107911.
- 26. M. Mathapati, K. Amate, C. Durga Prasad, M.L. Jayavardhana, and T. Hemanth Raju, Materials Today: Proceed. 50 (2022) 1535-1540.
- G.G. Carette and V.M. Malhotra, in Energy, Mines and Resources Canada, Ottawa, on, canmet Report 86-6E. (1986).
- F.E. Huggins, Intern. J. Coal Geo. 50[1-4] (2002) 169-214.
- H.L. Jacobs and J. Bennett, Source: Sewage and Industrial Wastes 22[9] (1950) 1207-1213.
- W. Xiulan, H. Zhezhe, R. Qiang, L. Huanhuan, L. Fei, and W, Tengyue, J. Alloys and Compounds 702 (2017) 442-448.
- B. Manisha, P. Manish, P.B.S. Bhadoria, and S.C. Mahapatra, Progress in Natural Sci. 19 (2009) 1173-1186.
- 32. T.K. Mukhopadhyay, S. Ghosh, J. Ghosh, S. Ghatak, and H.S. Maiti, Ceram. Intern. 36 (2010) 1055-1062.
- N. Bouzoubaa, M.H. Zhang, and V.M. Malhotra, Cem. Concr. Res. 30 (2000) 1037-1046.
- R.O. Lane and J.F. Best, Concrete Inter. 4[7] (1982) 81-92.
- 35. H.Y. Aruntas, Department of Construction Education,

- Faculty of Technical Education, Gazi University, Technical Schools Ankara 21[1] (2006) 193-203.
- M. Erol, S. Küçükbayrak, and A.E. Meriçboyu, J. Hazardous Mater. 153[1-2] (2008) 418-425.
- A.Ç. Öztürk PhD Thesis (Mimar Sinan University, Institute of Science Edirne 2001) 107.
- A. Mir Akbar, "Industrial waste" (in: E. James, Alleman, T. Joseph, Kavanagh (Eds.) Proc. 14th Mid-Atlantic Conf, Am. Arbor Science Publishers Ann Arbor 1982) MI.
- 39. N.U. Kockal, Ceram. Vidr. 51 (2012) 297-304.
- S.K. Das, S. Kumar, K.K. Singh, and P.R. Rao (in: Proceedings of the National Seminar on RVBIS, held in Ghatsila, India IIM 1996) p.7.
- 41. S. Kumar, K.K. Singh, and P.R. Rao, J. Mater. Sci. 36 (2001) 5917-5922.
- 42. W. He and X.D. Zhang (in: Proceedings of the 4th European Ceramic Society Conference Floor and wall tiles Riccione Spain October 1995) p.111.
- A. Manoshi, V. Rosouli, M. Mastali, and A. Kazami (in: Proceedings of the 4th European Ceramic Society Conference Floor and Wall Tiles Riccione, Spain 1995) p.85.
- 44. J.H. Zhang, T.C. Lee, and W.S Lau, J Mater Process Technol, 63 (1997) 908-912.
- M.H. Chen, L. Gao, J.H. Zhou, and M. Wang, J. Mater. Process. Technol. 129 (2002) 408-411.
- 46. O. Aguilar-García, S. Bribiesca-Vazquez, and J. Zárate-Medina, J. Ceram. Process. Res. 10[1] (2009) 37-42.
- 47. Salem, S.H. Jazayeri, E. Rastelli, and G. Timellini, J. Ceram. Process. Res. 10[5] (2009) 621-627.
- 48. N. Ediz and A. Yurdakul, J. Ceram. Process. Res. 10[4] (2009) 414-422.
- 49. N. Ediz and A. Yurdakul, J. Ceram. Process. Res. 10[6] (2009) 758-769.
- 50. F.A. Firat, J. Ceram. Process. Res. 13[6] (2012) 756-761.
- Z.B. Ozturk and N. Ay, J. Ceram. Process. Res. 13[5] (2012) 635-640.
- Z.B. Ozturk, J. Ceram. Process. Res. 17[6] (2016) 555-559.
- J. Song, X. Yang, P. Chen, H. Xu, D. Luo, R. Liu, and Z. Lai, J. Ceram. Process. Res. 23[4] (2022) 409-414.
- H. Yildizay, J. Ceram. Process. Res. 24[2] (2023) 237-241.
- T. Boyraz and A. Akkuş, J. Ceram. Process. Res. 22[2] (2021) 226-231.
- H. Wang, Z. Mengguang, S. Yongqi, J. Ru, L. Lili, and W. Xidong, Const. Build. Mater. 155 (2017) 930-938.
- L. Yang, Z. Shili, M. Shuhua, L. Chunli, and W. Xiaohui, Ceram. Intern. 43[15] (2017) 11953-11966.
- 58. K. Dana, J. Dey, and S.K. Das, Ceram. Intern. 31 (2005) 141-152.
- S. Basin, S.S. Amritphale, and N. Chandra, Br. Ceram. Trans. 102[2] (2003) 83-86.
- S.K. Das, S. Kumar, K.K. Singh, and P.R. Rao (in: Proceedings of the National Seminar on RVBIS, held in Ghatsila India Published by IIM 1996) p.7-10.
- H.M. Shah and K.N. Maiti, Trans. Ind. Ceram. Soc. 60[3] (2001) 145-149.
- P. Türker, B. Erdoğan, F. Katnaş, and A. Yeğinobalı, TÇMB (2004) Ankara.